CHAPTER 2

Sensitivity, Selectivity, and Stability of Gas-Sensitive Metal-Oxide Nanostructures

V. E. Bochenkov, G. B. Sergeev

Laboratory of Low Temperature Chemistry, Department of Chemistry, M. V. Lomonosov Moscow State University, Moscow 119991, Russia

CONTENTS

1. Introduction 32
   1.1. Definition and Classification 32
   1.2. Characteristics of Gas Sensors 33
2. Metal-Oxide Gas Sensors 34
   2.1. Historical Background 34
   2.2. Structure of the Sensing Layer 34
   2.3. The Nature of Gas Sensitivity in Semiconductor Metal Oxide Nanomaterials 35
   2.4. Factors Affecting the Sensitivity of Metal-Oxide Gas Sensor Materials 37
   2.5. Selectivity 40
   2.6. Stability of Metal Oxide Gas Sensors 41
3. Properties and Applications of Nanostructured Metal Oxides 42
   3.1. Detection of Hydrocarbons 42
   3.2. Detection of Alcohols 43
   3.3. Detection of Carbon Oxides 44
   3.4. Detection of Nitrogen Oxides 45
   3.5. Detection of Hydrogen 46
   3.6. Detection of Ammonia 47
   3.7. Detection of Other Gases 48
4. Conclusions and Future Directions 48
   References 48

ISBN: 1-58883-176-0

Metal Oxide Nanostructures and Their Applications
Edited by Ahmad Umar and Yoon-Bong Hahn
Volume 3: Pages 31–52

1. INTRODUCTION

1.1. Definition and Classification

According to the definition of a gas sensor, given by the International Union of Pure and Applied Chemistry (IUPAC), "a chemical sensor is a device that transforms chemical information, ranging from the concentration of a specific sample component to total composition analysis, into an analytically useful signal. The chemical information, mentioned above, may originate from a chemical reaction of the analyte or from a physical property of the system investigated" [1]. Typically, chemical sensors consist of two main parts, a *receptor* and a *transducer*. The receptor transforms chemical information into a form of energy, which can be measured by the transducer. The transducer converts this energy into a useful, typically electrical, analytical signal.

Chemical sensors are classified in a number of different ways. One of the classifications uses the operating principle of the receptor [1]. Using this principle, one can distinguish between

- physical sensors,
- chemical sensors, and
- biochemical sensors.

In physical sensors no chemical reaction takes place at the receptor, and the signal is a result of a physical process, such as mass, absorbance, refractive index, temperature, or conductivity change. Chemical sensors are based on chemical reactions between analyte molecules and the receptor. Biochemical sensors are a subclass of chemical sensors, where the reaction is biochemical. Typical examples of such sensors are microbial potentiometric sensors or immunosensors. It is not always possible to discriminate between physical and chemical sensors. A good example is a gas sensor, where the signal is a result of gas adsorption.

Chemical sensors can be classified according the operating principle of the transducer. An example of such classification is presented in Table 1.

A number of other classification schemes can be based on the type of sensitive material (e.g., metal-oxide, polymeric, and inorganic), fabrication technology (e.g., screen-printed and vapor deposited), field of application (automotive, medicine, and environmental), and so on. This chapter mainly discusses the features of metal-oxide gas sensors and

Table 1. Classification of chemical sensors by transducer operating principle.

Transducer operating principle	Measured properties	Source of signal
Optical	Absorbance	Either caused by analyte itself, or due to reaction with certain indicator
	Fluorescence	Changes in fluorescence properties
	Luminescence	Emission, caused by chemical reaction
	Refractive index	For example, caused by change in solution composition
	Scattering	Caused by particles of definite size present in the sample
Electrochemical	Voltammetric	Change of current is measured. For example, chemically inert, active and modified electrodes
	Potentiometric	Change of electrode potential is measured against a reference electrode
Mass	Piezoelectric	Changes of resonant frequency of quartz oscillator plate due to adsorption of an analyte on its chemically modified surface
	Acoustic wave	Changes of propagation velocity of acoustic wave
Magnetic	Paramagnetic	For example, oxygen monitors
Calorimetric	Heat effects	Changes of temperature due to heat effects of reaction or adsorption

presents their sensing mechanisms. The main sensor characteristics and the approaches for their improvement are considered. The modern results and future prospects of using nanotechnology with its ability to precisely control the structure of the sensitive layers in order to affect sensor performance are reviewed.

1.2. Characteristics of Gas Sensors

In order to characterize sensor performance a set of parameters is used [2]. The most important parameters and their definitions are listed below.

- *Sensitivity* is a change of measured signal per analyte concentration unit, i.e., the slope of a calibration graph. This parameter is sometimes confused with the detection limit.
- *Selectivity* refers to characteristics that determine whether a sensor can respond selectively to a group of analytes or even specifically to a single analyte.
- *Stability* is the ability of a sensor to provide reproducible results for a certain period of time. This includes retaining the sensitivity, selectivity, response, and recovery time.
- *Detection limit* is the lowest concentration of the analyte that can be detected by the sensor under given conditions, particularly at a given temperature.
- *Dynamic range* is the analyte concentration range between the detection limit and the highest limiting concentration.
- *Linearity* is the relative deviation of an experimentally determined calibration graph from an ideal straight line.
- *Resolution* is the lowest concentration difference that can be distinguished by sensor.
- *Response time* is the time required for sensor to respond to a step concentration change from zero to a certain concentration value.
- *Recovery time* is the time it takes for the sensor signal to return to its initial value after a step concentration change from a certain value to zero.
- *Working temperature* is usually the temperature that corresponds to maximum sensitivity.
- *Hysteresis* is the maximum difference in output when the value is approached with an increasing and a decreasing analyte concentration range.
- *Life cycle* is the period of time over which the sensor will continuously operate.

All of these parameters are used to characterize the properties of a particular material or device. An ideal chemical sensor would possess high sensitivity, dynamic range, selectivity and stability; low detection limit; good linearity; small hysteresis and response time; and long life cycle. Investigators usually make efforts to approach only some of these ideal characteristics, disregarding the others. On one hand, this is because the task of creating an ideal sensor for some gases is extremely difficult, if at all possible. On the other hand, real applications usually do not require sensors with all perfect characteristics at once. For example, a sensor device monitoring the concentration of a component in industrial process does not need a detection limit at the ppb level, though the response time at range of seconds or less would be desirable. In case of environmental monitoring applications, when the concentrations of pollutants normally change slowly, the detection limit requirements can be much higher, but response time of a few minutes can be acceptable.

The first section of this chapter is devoted to the definition and classification of gas sensors, and a discussion of factors affecting the sensitivity and selectivity of metal-oxide based sensors. Attention is paid to the structure and conductivity of the surface layer, the size- and shape-dependence of the sensitivity of the oxide particles, and the influence of doping on gas sensor characteristics. The second section discusses the applications of such metal-oxide nanostructures as SnO_2, ZnO, and WO_3 and their combinations for analysis of hydrocarbons, toxic oxides of carbon, and nitrogen and for detection of alcohols and some other volatile organic compounds.

2. METAL-OXIDE GAS SENSORS

2.1. Historical Background

It has been known for a long time that electrical resistance of a semiconductor is very sensitive to the presence of impurities in its volume or at the surface. In 1953, this effect was demonstrated for Ge [3]. Later, it was shown that the conductivity of ZnO thin films heated to ~300°C was sensitive to the presence of traces of reactive gases in the air [4]. Similar properties were reported for SnO_2, with higher stability [5]. These results initiated further development of commercial gas sensors.

The early metal oxide-based sensor materials possessed a number of unpleasant characteristics, such as high cross-sensitivity, sensitivity to humidity, long-term signal drift and, slow sensor response. In order to improve sensor performance, a series of various metal-oxide semiconductors have been tested [6]. At first, the poor understanding of sensor response mechanisms caused the use of trial and error strategy in the search of an appropriate material. The most successful investigations were connected with SnO_2, ZnO, and TiO_2. Parallel to this approach, the basic research of metal-oxide materials was carried out in scientific laboratories.

Several decades after the first published paper on SnO_2 sensors, they became the best-understood prototype of oxide-based gas sensors. It was well known that the sensor characteristics can be changed by varying the crystal structure, dopants, preparation technology, operation temperature, etc. Nonetheless, highly specific metal-oxide sensors were still not available. In recent years, the interest of researchers and engineers to gas-sensitive materials has grown substantially due to the progress in nanotechnology. This interest is primarily connected to the promising electronic properties of nanomaterials: their size-dependence and ability to control the material structure by new experimental techniques [7]. More and more materials and devices are produced every year with the use of nanotechnology [8–10].

2.2. Structure of the Sensing Layer

The typical metal-oxide gas sensor element consists of the following parts:

- sensitive layer,
- substrate,
- electrodes, and
- heater.

Today, most of the commercial metal-oxide gas sensors are manufactured by screen printing on small and thin ceramic substrates. The advantage of this preparation technique is that the thick films of metal oxide semiconductor can be deposited in batch processing, leading to small deviations of characteristics for different sensor elements.

Although this fabrication technology is well-established, it possesses a number of drawbacks and needs to be improved. Primarily, the drawbacks are connected with the necessity to keep the thick metal oxide film at high temperature. Due to this reason the power consumption of screen-printed sensors can be as high as 1 W [11], which makes them unable to be used in battery-driven devices. Another technological problem is the proper mounting of the overall hot ceramic plate to ensure the good thermal isolation between the sensor element and housing.

These problems have promoted the development of substrate technology and strong research in preparation of the sensitive layer. One promising solution is the integration of a sensing layer in standard microelectronic processing, which overcomes the difficulties of the screen-printed sensors. In this case, an oxide layer is deposited onto a thin dielectric membrane of low thermal conductivity, which provides good thermal isolation between the substrate and the heated area on the membrane. Such a construction allows the power consumption to be kept at very low levels [11]. Moreover, the total size of single sensor elements is reduced, so that a minimal distance between electrodes lying in the μm range can be achieved. It enables the integration of signal-processing electronics and/or multiple sensor elements on the same substrate.

2.3. The Nature of Gas Sensitivity in Semiconductor Metal Oxide Nanomaterials

The change of electrical properties of the metal-oxide semiconductor due to adsorption of gas molecules is primarily connected with the chemisorption of oxygen. Molecular oxygen adsorbs on the surface by trapping an electron from the conduction band of the semiconductor. At temperatures between 100 and 500°C the ionized molecular (O_2^-) and atomic (O^-, O^{2-}) forms can be present at the surface [12]. The molecular form dominates below 150°C, whereas above this temperature, ionic species prevail [13, 14]. The general reaction equation can be written as:

$$\frac{\beta}{2}O_2^{(gas)} + \alpha \cdot e^- + S \longleftrightarrow O_{\beta(S)}^{\alpha-} \tag{1}$$

Here $O_2^{(gas)}$ is an oxygen molecule in the ambient atmosphere and e^- is an electron that can reach the surface, overcoming the electric field resulting from negative charging of the surface. Their concentration is n_s. S denotes unoccupied chemisorption sites for oxygen, $O_{\beta(S)}^{\alpha-}$ is the chemisorbed oxygen with $\alpha = 1$ or 2 for singly or doubly ionized form and $\beta = 1$ or 2 for atomic or molecular form, respectively. The presence of charged species on the surface of a semiconductor induces band bending and formation of a depletion layer [15, 16]. Depending on the type of semiconductor the concentration of charge carriers in the surface layer can be either increased or decreased. The space charge layer is described by the thickness L_S and surface potential (V_S) [17, 18].

The conductance dependence can be found following the derivation given in Ref. [13]. The mass action law can be written in the form:

$$k_{ads}[S]\, n_S^{\alpha} p_{O_2}^{\beta/2} = k_{des}\left[O_{\beta(S)}^{\alpha-}\right] \tag{2}$$

Let us denote the total concentration of the oxygen adsorption sites (occupied and unoccupied) as $[S_t]$, so that $[S_t] = [S] + [O_{\beta(S)}^{\alpha-}]$. By definition the surface coverage is

$$\theta = \frac{\left[O_{\beta(S)}^{\alpha-}\right]}{S_t} \tag{3}$$

Equation (2) can be than rewritten:

$$(1-\theta)k_{ads}n_s^{\alpha}p_{O_2}^{\beta/2} = k_{des}\theta \tag{4}$$

Since electron concentration n_s and surface coverage θ are related, an additional equation is needed to find the dependence of n_s with partial oxygen pressure. One can use the electroneutrality equation combined with the Poisson equation.

The electroneutrality principle in the Schottky approximation states that the charge in the depletion layer L_S under surface A equals to the charge captured by surface A. The usual working temperature of metal-oxide sensors is high enough to assume that all donors are ionized, so the ionized donor concentration is equal to the bulk electron density n_b. Therefore one can write the electroneutrality equation

$$\alpha \cdot \theta \cdot [S_t] \cdot A = n_b \cdot L_S \cdot A \tag{5}$$

and the Poisson equation for energy E as follows:

$$\frac{d^2E(z)}{dz^2} = \frac{q^2 n_b}{\varepsilon\varepsilon_0} \tag{6}$$

Setting boundary conditions to

$$\frac{dE(z)}{dz}\Big|_{z=L_S} = 0 \tag{7}$$

and

$$E(z)\big|_{z=l_S} = E_C \tag{8}$$

results in Eq. (9):

$$E(z) = E_C + \frac{q^2 n_b}{2\varepsilon\varepsilon_0}(z - z_0)^2 \tag{9}$$

which leads to the dependence of band bending, given that $V = E/q$:

$$V(z) = \frac{qn_b}{2\varepsilon\varepsilon_0}(z - z_0)^2 \tag{10}$$

This general dependence allows surface band bending (at $z = 0$):

$$V_S = \frac{qn_b}{2\varepsilon\varepsilon_0} z_0^2 \tag{11}$$

By combining this equation with electroneutrality equation [Eq. (5)] and taking into account the following relation

$$n_s = n_b \exp\left(-\frac{qV_S}{kT}\right) \tag{12}$$

one obtains Eq. (13). In combination with Eq. (4) it allows determination of n_s and θ as a function of oxygen partial pressure and temperature either numerically or by using various approximations.

$$\theta = \sqrt{\frac{2\varepsilon\varepsilon_0 n_b kT}{\alpha^2 [S_t]^2 q^2} \cdot \ln\frac{n_b}{n_s}} \tag{13}$$

For granular metal oxides, the formation of a depletion layer at the surface of grains and grain boundaries leads to the formation of Schottky barriers between the oxide crystallites, as depicted in Figure 1. The density of surface oxygen ions and the height and width of Schottky barriers depend on the oxygen partial pressure in the surrounding atmosphere. The electronic theory of adsorption [16] is in quantitative agreement with the experimentally observed conductance dependencies of semiconductor layers on oxygen partial pressure [19].

Depending on the content of the atmosphere, the concentration of the surface oxygen ions—and therefore the occupation of the surface states—can be changed, leading to the

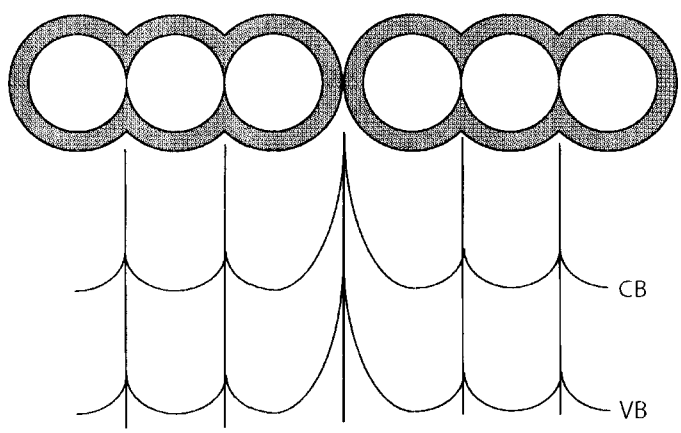

Figure 1. Schematic representation of barrier formation at the grain boundaries due to the space charge layer. The shaded part denotes the space charge region (high resistivity); the un-shaded part denotes the core region (low resistivity). CB and VB are the lowest edge of the conduction band and the highest edge of the valence band, respectively.

change in conductivity. As a measure of gas sensitivity one can use either the conductivity change of the sample, exposed to the analyte-containing atmosphere in relation to its conductivity in the reference gas, or the slope of the dependence of conductivity on analyte concentration [20].

2.4. Factors Affecting the Sensitivity of Metal-Oxide Gas Sensor Materials

As mentioned above, the requirements for each gas sensor depend on the particular application. It is not necessary to have material with a detection limit of one molecule if the sensor is designed to work in the 1–10% concentration range. Nonetheless, materials with high sensitivity and low detection limit always attract the attention of scientists and engineers. In this section, the main approaches for increasing the gas sensitivity of metal-oxide sensor materials are listed, namely those utilizing the size effects and doping by metal or other metal oxides.

2.4.1. Size and Shape Effects

Since during the formation of a space charge layer the carrier concentration in volume is decreased only in thickness L_S, three types of conductance mechanisms, as illustrated in Figure 2 can be realized. For large crystallites the grain size $D \gg 2L$, and the conductance of the film is limited by Schottky barriers at grain boundaries. In this case, the sensitivity is practically independent of D. When grain size is comparable to $2L$ ($D = 2L$) every conducting channel in the necks between grains becomes small enough to influence the total conductivity. Since the number of necks is much larger the grain contacts, they govern the conductivity of the material and define the size-dependence of gas sensitivity. If $D < 2L$, every grain is fully involved in the space charge layer, and the electron transport is affected by the charge on the particles' surfaces.

The considered Schottky barrier formation model was developed for the semi-infinite planar geometry system. It can be safely used to describe the barrier formation in case of large metal-oxide grains. However, for materials with the grain sizes comparable to the length of the depletion region, the effect of the curvature cannot be neglected, since the density of surface states depends on the grain radius [21, 22].

The shape of a bottom of conductive band for the grains of different size was studied theoretically. Application of the depletion approximation (DA) under spherical symmetry allowed the calculation of an an analytical solution for the potential $P(r) = (E_{Cb}(r))/q$, where $E_{Cb}(r)$ is the energy of the bottom of of the conductive band at a distance r from the center of a grain. For a more general case, where DA is not applicable, the Poisson equation using a complete expression for the charge density can be solved only numerically. The calculated potential shape inside the grains agrees with the experimentally observed flattening of the band bending for films in air [21, 23]. Thus, by reducing the

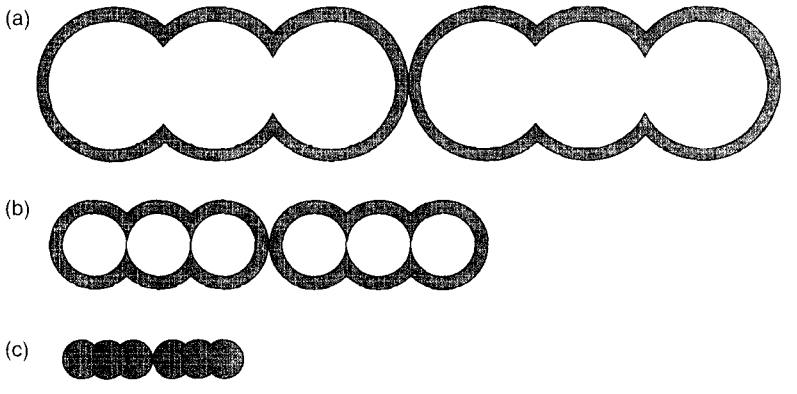

Figure 2. Three mechanisms of conductance in metal-oxide gas-sensitive materials. The shaded part shows the space charge region (high resistivity), while the un-shaded part shows the core region (low resistivity). (a) $D < 2L$, grain boundary control; (b) $D < 2L$, neck control; (c) $D < 2L$, grain control.

particle size the conduction of the sample may be controlled by the grain boundaries, necks, or grains. The latter case is the most desirable, since it allows achieving the highest resistance change. For different semiconductor oxides the length of depletion layer may vary in the range of 1–100 nm. Numerous experimental investigations of nanostructured metal-oxide films revealed a strong increase in sensitivity when the average grain size was reduced to several nanometers [5, 24–27]. Systematic analysis of size-dependence of SnO_2 sensitivity was presented recently [28].

Another prospective approach is to affect the sensitivity by changing the microstructure and porosity. For this purpose the low-temperature vapor co-deposition of metal and inert gas can be used. After removing the gas by annealing, the highly porous metal structure can be formed. Then, metal can be oxidized by reaction with oxygen. This approach was used for preparation of porous Pb/PbO nanostructures by co-deposition of Pb vapors with CO_2 at 80 K followed by annealing [29]. SnO_2 and TiO_2 mesoporous powders fabricated using a self-assembly of a surfactant followed by treatment with phosphoric acid as well as conventional tin oxide powders with surfaces modified by mesoporous SnO_2 show higher sensor performance than corresponding metal-oxide powder materials, which have lower specific surface area [30, 31]. Other porous metal oxides also exhibit increased gas sensitivity [32–34].

In recent years, a definite trend in using quasi one-dimensional (1D) nano-objects for gas sensor applications has been observed [7, 35–39]. This is due partly to expanding opportunities for synthesis and characterization of such structures [40, 41]. Besides, the application of nanowires, nanorods, nanobelts, and nanotubes for gas sensors can significantly lower the detection limit, since the conductance of 1D objects is affected by lower amounts of adsorbed analyte than is the case for thin granular films. It was found that SnO_2 nanowires are sensitive to low CO concentrations [42–44], so the gas sensitivity of SnO_2 nanobelts (the quasi-1D materials with defined crystal structure) to polluting gases like CO, NO_2, and ethanol was tested [35, 37, 45].

An additional increase of sensitivity can be achieved by creating 1D objects with necks that define the conductivity of the whole nano-object. The comparative study of the sensor response to 0.4 ppm of hydrogen of straight SnO_2 nanowires with diameter of ~100 nm and segmented nanowires consisting of thick parts 500 nm in diameter connected by thin parts 10 nm in diameter [46] was carried out. It was found that response is larger for segmented nanowires, despite the fact that their mean radius is almost three times larger than that of straight nanowires.

2.4.2. Doping

The sensitivity of metal-oxide gas sensors can be substantially improved by dispersing a low concentration of additives, such as Pd [47, 48], Pt [49], Au [50, 51], Ag [28, 52, 53], Cu [54], Co [55], and F [56] on oxide surface or in its volume. Although doping has been used for a long time now in preparation of commercial gas sensors, the working principle of additive-modified metal-oxide materials is still not completely understood. Two general schemes of the gas sensing mechanism are depicted in Figure 3. In the chemical scheme (Fig. 3(a)) the reaction takes place at the oxide surface. The role of the additive nanoparticles is considered within a spillover process, increasing the metal-oxide

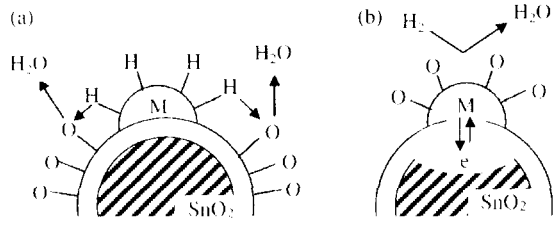

Figure 3. Chemical (a) and electronic (b) sensitization schemes in metal-doped SnO_2 gas sensor. Reprinted with permission from [7], V. E. Bochenkov and G. B. Sergeev, *Adv. Coll. Int. Sci.* 116, 245 (2005). © 2005, Elsevier Limited.

surface coverage of the gas, involved in the sensing scheme. In the electronic mechanism (Fig. 3(b)) the reaction involves the dopant atoms, and the oxide material has to transduce the electrochemical changes into a detectable output signal. Moreover, the introduction of additives may lead to the formation of new donor or acceptor energy states or influence the grain size and growth mechanism [57].

The chemical scheme is usually considered in the case of catalytic additives, for example Pt- or Pd-doped SnO_2 material exposed to hydrogen, hydrocarbons, or carbon monoxide [58–60]. It is supposed that the reduction of gas molecules is first activated by the metal surface, forming the active surface species that then react via a spillover process with the charged oxygen molecules, adsorbed on tin oxide. This reaction leads to the re-injection of the localized electrons back to the bulk, thus increasing the conductivity of the material. For instance, the sensing mechanism proposed for the $Pt/SnO_2 + CO$ system involves two main processes [58]. First, at elevated temperature, Pt is oxidized by the chemisorbed oxygen:

$$Pt + 2O_{ads} \rightarrow PtO_2 \tag{14}$$

Second, exposure to CO leads to a reduction of platinum oxide:

$$PtO_2 + 2CO \rightarrow Pt + 2CO_2 \tag{15}$$

The analysis of published papers on doped metal oxide gas sensors shows the increase of such works in recent years. The results of a literature search using the words "metal oxide AND gas sensor AND doped" in title, keywords, and abstract are presented in Figure 4.

Though the search criteria do not allow the values presented in Figure 4 to be considered as precise number of papers using doped metal oxide materials as gas sensors, it gives some ideas of the existing trends. Data on year 2007 are not included, since the information about recently published papers could be unavailable at the moment of preparation of a given manuscript. The variety of elements used for doping the metal oxides is noteworthy. The diagram, presenting the relative comparison of dopants, used for enhancing properties of SnO_2 gas sensors in recent years, is depicted in Figure 5

The most often used dopant for SnO_2 gas sensors is palladium due to its well known catalytic properties. A similar situation is observed for other metal-oxide gas sensors. Another popular doping element is copper. It was found that the doping of SnO_2 with Cu enhances the sensitivity and selectivity to H_2S [61–63]. The same effect was observed for $CuO–SnO_2$ [64, 65] and $SnO_2–CuO–SnO_2$ [66] heterostructures. This phenomenon is

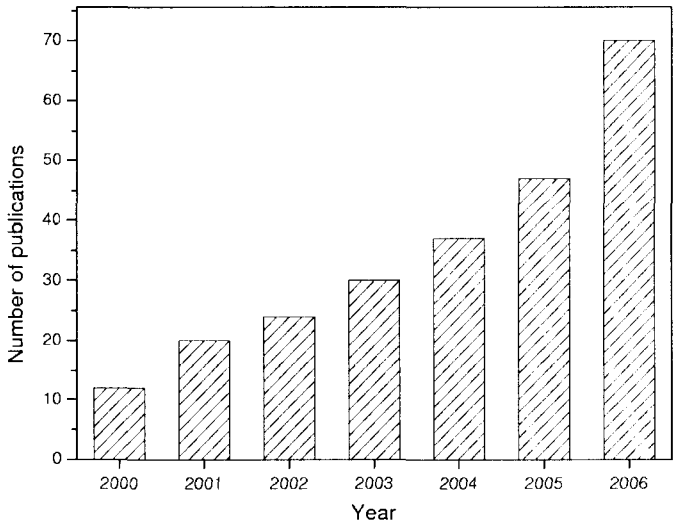

Figure 4. Number of publications having the words "metal oxide," "gas sensor," and 'doped' in the title, abstract, or keywords.

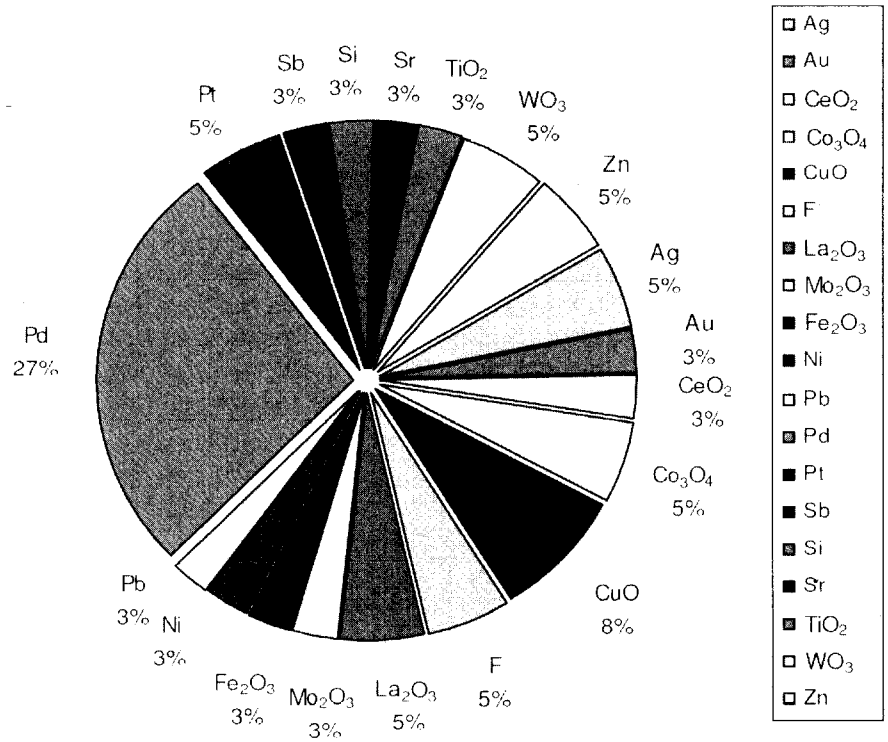

Figure 5. Relative comparison of dopants for SnO_2 gas sensors.

explained by the decreasing barrier height in *p*-CuO–*n*-SnO_2 due to the chemical transformation of highly resistive CuO into good-conducting Cu_2S. Thorough studies have shown that the copper atoms in Cu-doped SnO_2 can form donor-like sites, which possess much better stability than the intrinsic donors (oxygen vacancies) in pure SnO_2 [67]. Doping by metal nanoparticles affects not only the sensitivity, but also the selectivity of the metal-oxide gas sensors.

2.5. Selectivity

One of the main challenges to the developers of metal-oxide gas sensors is high selectivity. Currently, two general approaches exist for enhancing the selective properties of sensors. The first one is aimed at preparing a material that is specifically sensitive to one compound and has low or zero cross-sensitivity to other compounds that may be present in the working atmosphere. To do this, the optimal temperature, doping elements, and their concentrations are investigated. Nonetheless, it is usually very difficult to achieve an absolutely selective metal oxide gas sensor in practice, and most of the materials possess cross-sensitivity at least to humidity and other vapors or gases.

Another approach is based on the preparation of materials for discrimination between several analytes in a mixture. It is impossible to do this by using one sensor signal; therefore, it is usually done either by modulation of sensor temperature [68–74] or by using sensor arrays [75–77]. In the former case, such discrimination is possible because of the different adsorption and reactivity properties of analytes. In the latter case, N signals are obtained simultaneously from N sensors, which usually differ in some way (e.g., doping element, doping ratio, grain size, or temperature). These kind of devices are usually referred to as "electronic noses." In both cases, signals are typically analyzed by an artificial neural network.

2.5.1. Modulation of Temperature

Typically, temperature dependence of a metal-oxide sensor signal to the presence of a given analyte possesses a bell shape with a maximum at a certain temperature [78].

This dependence arises due to several reasons. First of all, as mentioned above, the charge of oxygen species adsorbed at the oxide's surface depends on temperature [12]. Second, since the oxidation reaction is an activated process, its rate increases with temperature. Finally, all adsorption, desorption, and diffusion processes are temperature-dependent [79]. Thus, temperature modulation leads to response patterns that are characteristic of the species present in a gas mixture [80]. This allows measuring of multivariate information from every single sensor. An appropriate extraction of this information helps improve selectivity [81]. For example, a dynamic measurement method for the rapid identification and determination of volatile organic compounds (VOCs) in ambient air using a single SnO_2-based gas sensor was developed [73]. The sensor operated in a rectangular temperature-modulation mode. The working temperature of the sensor was modulated between 250 and 300°C. It was shown that the discrete wavelet transform allows important features to be extracted from the sensor response. These features can then be processed using a pattern recognition algorithm. The species considered can be discriminated with a 100% success rate using a back propagation network, and the concentrations of the organic vapors can also be accurately predicted.

Nonlinear responses of SnO_2 sensors to alcohol vapors and hydrocarbons were found to depend characteristically on the scanning profile of the cyclic temperature change [70]. This allowed an increase in the selectivity to target analytes. The temperature was regulated by the second-harmonic heater voltage to improve the discrimination of the nonlinear dynamic response. The phase of the second-harmonic heater voltage can partially change the dynamic sensor response, which depends on the kinetics of gases on the sensor surface. The dynamic responses of a semiconductor gas sensor under the application of a temperature variation including the second harmonic were characterized by the higher harmonics of fast Fourier transformation (FFT).

Small temperature variations of a nanoparticular SnO_2 gas sensor were reported to allow differentiation between different gas mixtures at a ppm level [69]. Thus, different concentrations of CO (from 50 to 200 ppm) were well differentiated even at high C_3H_8 and NO_2 concentrations. It was shown that the shapes of transient responses can be modified by adding different catalysts (Pt, Pd) in an SnO_2 sensing layer.

2.5.2. Sensor Arrays

The sensor arrays are named "electronic noses" due to the parallel between the measurement concept of the instrument and that of the mammalian olfactory system. In the latter, during sniffing, the volatile compounds reach the receptors located in the upper nasal cavity. Electrical stimuli produced by the receptors are transmitted by neurons to the brain, where the pattern recognition process takes place with the help of memory. Electronic noses operate using a similar principle: the signals from different semi-selective sensors form signals, which are then analyzed by an artificial neural network program. Similar aromas generally result in similar sensor response patterns. Many approaches exist for making the array elements in a single sensor possess different sensitivities to various analytes, including doping with different chemical elements [82, 83], formation of grains using various mixed oxides [84], and applying the temperature gradient over the sensor array [76, 85]. The current status of the development of electronic nose systems was reviewed recently [77, 86].

2.6. Stability of Metal Oxide Gas Sensors

Another issue of metal-oxide gas sensor materials is their low stability and long-range signal drift. This problem leads to in uncertain results, false alarms and the need to frequently recalibrate or replace sensors. Little attention is paid in the literature to the problems of stability. Only a few papers, cited in this chapter, report the stability of sensor response in a period of several days [87].

Generally, nanostructured oxides with small grains as well as nanotubes, nanorods etc. are subject to degradation because of their high reactivity. There is no unified approach to increasing the stability of metal-oxide gas sensors. To some extent, stability can be

increased by calcination and annealing as the post-processing treatment and by reducing the working temperature of the sensor element. Doping metal oxides with metal particles or carbon nanotubes as well as synthesis of mixed oxides have been also reported to increase the stability of sensor elements [88, 89].

One can distinguish between the two types of sensor stability. One is connected with reproducibility of sensor characteristics during a certain period of time at working conditions, which may include high temperature and the presence of a known analyte. Such stability may be referred to as active stability. Another type of sensor stability, which can be called conservative stability, is connected with retaining the sensitivity and selectivity during a period of time at normal storage conditions, such as room temperature and ambient humidity.

3. PROPERTIES AND APPLICATIONS OF NANOSTRUCTURED METAL OXIDES

In this section, more concrete examples of metal-oxide sensor development will be presented. The material is subdivided by target analyte compounds, discussing sensors for hydrocarbons, alcohols, carbon oxides, nitrogen oxides, hydrogen, ammonia and other gases. Each subsection contains a table citing some of the recent papers with indication of the sensor material, working temperature, and the analyte and concentration that are detectable by given sensors. It can be as the detection limit, so as the dynamic range or just one concentration used by authors to measure the sensitivity of synthesized material. Since the various types of metal-oxide gas sensors and their applications for detection of various gases and volatile organic compounds are numerous, we will discuss only some examples that are notable from our point of view.

3.1. Detection of Hydrocarbons

In recent years, metal oxides have been widely used for analysis of hydrocarbons. Sensors for some aliphatic and aromatic hydrocarbons have been developed, and attention has been paid to the detection of volatile liquid as well as gaseous compounds. Some recent works on hydrocarbons sensors are presented in Table 2.

The application of metal oxides to the detection of hydrocarbons is reviewed here using the example of methane, the first member of the aliphatic row. Methane is widespread in nature and forms explosive mixtures with air. Therefore, the development of cheap gas sensors for detection of methane and small hydrocarbons is an important problem.

The application of thin zinc oxide films with contacts made of noble metals for detection of methane is described in papers [95, 98]. Thin nanocrystalline films of ZnO were deposited on a 0.6 μm-thick SiO_2-coated p-Si substrate by a sol–gel method. The thickness of ZnO films was about 900 nm. The contacts of different metals (Pd–Ag, Rh, and Pt) were deposited using an e-beam evaporator. The shortest response time (16 s) was found for Pd–Ag contacts, while the maximum response value (84%) was observed in case of Rh contacts at 250°C.

Table 2. Some recent works on detection of hydrocarbons.

Material	Analyte	Concentration	Temperature (°C)	Ref.
ZnO	C_3H_6	0–200 ppm	600	[90]
ZnO:Al	C_3H_8	5,000 ppm	350	[91]
ZnO:Au	C_4H_{10}	1,000 ppm	Room temp.	[92]
ZnO	C_4H_{10}	1,000 ppm	300	[93]
SnO_2	CH_4	500–10,000 ppm	350	[94]
ZnO	CH_4	0.5–1%	50–350	[95]
ZnO	CH_4	0.1–1%	30–350	[96]
SnO_2:WO_3	Ethylene	2–8 ppm	300	[97]

A proposed mechanism of sensor response involves dissociation of methane to a methyl group and a hydrogen atom followed by recombination of hydrogen atoms:

$$CH_{4(gas)} \longleftrightarrow CH_{3(ads)} + H_{(ads)} \quad (16)$$

$$2H_{(ads)} \longleftrightarrow H_{2(gas)} \quad (17)$$

The formed hydrogen molecule then reacts with adsorbed oxygen, producing H_2O and releasing trapped electrons to the conduction band of metal oxide semiconductor [99].

3.2. Detection of Alcohols

Sensor materials for detection of alcohols, especially ethanol, are being actively developed. The interest in ethanol is connected with its wide application in chemistry, medicine, and the food industry. Precise quantitative detection of ethanol vapors is required for determination of quality of wines and human health. Metal oxides are widely used for detection of ethanol. Ethanol sensors are being enhanced, and as is the case for other analytes, the problems of sensitivity, selectivity, and stability are being addressed. Some of the most recent papers on detection of alcohols are presented in Table 3.

The most widely used metal oxide materials for alcohol detection are SnO_2, ZnO, WO_3, TiO_2 and Zr_2O_3. As a rule, the analysis is carried out at temperatures above 400°C; therefore one important task is to decrease the operating temperature. Beside the conductivity measurements for sensor detection of alcohol vapors by metal oxides, the oxidation process can also be used. Oxidation of ethanol may lead to formation of acetaldehyde [118]. Oxidation of aldehyde is accompanied by photoluminescence, which is used for quantitative detection of alcohol.

Chemiluminescence caused by catalytic oxidation of ethanol vapors on zinc oxide has been analyzed [118]. Oxide nanoparticles were synthesized by a wet chemical method from $ZnSO_4$ and NH_4HCO_3 in the Triton X-100 solution followed by drying at 300°C and calcination at 600°C. Transmission electron microscopy showed that ZnO particles sizes were in range of 30–50 nm. By using X-ray powder diffraction data, the particles crystal structure were attributed to the wurtzite type. The sensitivity and its dependence on alcohol vapor flow rate and temperature as well as selectivity and lifetime were investigated by luminescence studies.

The sensor dynamic range was found to be 1–100 ppm, and the detection limit was estimated as 0.7 ppm. The optimal temperature for analysis was 358°C, and the optimal

Table 3. Some recent works on detection of alcohols.

Material	Analyte	Concentration	Temperature (°C)	Ref.
ZnO	Ethanol	ppb range	350	[100]
SnO_2:Pt	Ethanol	50–200 ppm	200	[101]
ZnO	Ethanol	500 ppb	400–500	[102]
ZnO	Ethanol	50 ppm	350	[103]
ZnO:Ga	Ethanol	50 ppm	300	[104]
SnO_2:Pd	Ethanol	4,000 ppm	350	[75]
ZnO:Al	Ethanol	400 ppm	250	[105]
ZnO	Ethanol	29.7 ppm	20	[106]
ZnO:Pd	Ethanol	25–250 ppm	400	[107]
ZnO	Ethanol	25–250	400	[108]
SnO_2:CeO_2	Ethanol	200 ppm	250–450	[109]
SnO_2/ZnO	Ethanol	200 ppm	300	[110]
ZnO:In	Ethanol	1–3 ppm	32	[111]
ZnO	Ethanol	125–250 ppm	400	[112]
ZnO:CeO_2	Ethanol	100 ppm	320	[113]
ZnO	Ethanol	0.5 ppm	400	[114]
ZnO	Ethanol	0.5 ppm	400	[115]
ZnO	Methanol, Ethanol	10 ppm	170	[116]
ZnO:Fe_2O_3, soot	Propanol	2,500–5,000 ppm	20	[117]

flow rate was 100 mL/min. High selectivity to 50 ppm of NH_3, N_2, CO_2, SO_2, CCl_4, C_6H_6 was reported. Stability of cataluminescence intensity measured at 460 nm was found to be stable after seven days, with RSD ($n = 7$) of about 3.5%. The analysis of artificial sample mixtures revealed good reproducibility and practically 100% recovery of the sensor [118].

Since ZnO can be prepared in a form of quasi-1D structure, a number of recent studies have been devoted to such materials. Thus, the influence of ZnO nanorod diameter on ethanol sensitivity was demonstrated [119]. Vertically-aligned nanorods with diameters 100, 200, 400, and 800 nm were prepared by reactive Zn vapor deposition in an oxygen-containing ambience on Si(100) substrate. The materials were exposed to air containing 100 ppm of ethanol at 100°C. Response and recovery times were about 10 s. The proposed sensing mechanism includes the chemisorption of oxygen and oxidation of the adsorbed ethanol molecule:

$$C_2H_5OH_{(ads)} + 6O^-_{(ads)} = 2CO_{2(gas)} + 3H_2O_{(l)} + 6e^- \quad (18)$$

The highest sensitivity was demonstrated on materials with the lowest ZnO nanorod diameter (100 nm). The authors suggested the reason is the higher surface-to-volume ratio, which promotes the adsorption of oxygen and higher concentration of lattice oxygen vacancies. It is noteworthy that the sensitivity of nanorods with diameters of 400 and 800 nm was practically equal.

We will briefly consider the most interesting peculiarities of alcohol sensors published in other papers without detailed analysis of all of them. Results similar to those discussed above on the ethanol sensitivity of ZnO nanorod sensor have been obtained at 350°C [100]. Aluminium-doped thin ZnO films, produced by radio frequency magnetron sputtering, showed sensitivity to of ~20–400 ppm of ethanol at 250°C [105].

Palladium-doped ZnO nanoparticles, produced by flame spray pyrolysis of organometallic precursors and mixed into an organic paste to form thick sensing films, were tested for detection of ethanol vapors in the 25–250 ppm range in dry air at 400°C. Dependence of sensitivity on Pd content [107] and film thickness [120] was studied. Pd content varied in the range of 0–5 mol%. The maximum sensitivity was found to correspond to 1 mol% of Pd. The thinnest sensing film (5 μm) showed the highest sensitivity and the fastest (within seconds) response time.

A lower concentration of ethanol was detected by CeO_2-doped ZnO thin films, fabricated using the dip-coating method [113]. The concentration of 100 ppm was detected with sensitivity of ~80 at 320°C by films containing 5% Ce. It was stated that the addition of Ce to ZnO modified the particle size distribution.

Highly porous three-dimensional (3D) networks of interconnected ZnO tetrapods, having legs with length of several micrometers and diameter in the 0.1–1 μm range, were found to be sensitive to ethanol concentrations as low as 0.5 ppm [114, 115, 121]. The response time was about 10 s at 400°C. The material was synthesized by heating Zn powder in a furnace at a temperature of 900°C and reaction with air and water vapor. The content of water vapor in air was found to control the adherence onto the substrate and the morphology of the deposited layers.

3.3. Detection of Carbon Oxides

Development of gas sensors for the detection of carbon monoxide is an issue of the day, since CO is one of the most toxic gases, and being odorless, it can form undetected by incomplete combustion of fuel in industry and in private houses. CO gas, which is contained in automobile exhaust along with nitrogen oxides, is one of the main environmental contaminants, especially in large cities. Another carbon oxide, CO_2, is one of the greenhouse gases, which are believed to be responsible for the global warming effect. The main source of CO_2 today is the combustion of fossil fuels. The number of papers devoted to development of new CO_2 sensor materials is rather small. Some recently developed sensor materials for CO and CO_2 are presented in Table 4 along with the references to the original papers.

Table 4. Some recent papers on detection of carbon oxides.

Material	Analyte	Concentration	Temperature (°C)	Ref.
SnO_2/TiO_2:Nb	CO	1,000 ppm	658–680	[122]
ZnO	CO	250 ppm	400	[91]
ZnO	CO	300 ppm	350	[123]
ZnO:Cu, Cr	CO	100 ppm	200, 300	[124]
ZnO	CO	50–1,000 ppm	250	[125]
SnO_2:Au	CO	10 ppm	250–300	[126]
SnO_2	CO	5 ppm	295	[44]
SnO_2:Pt	CO	5 ppm	400	[127]
ZnO	CO_2	100%	130	[128]

Development of new ZnO-based sensor materials for CO detection deals with preparation of new forms of oxide. 1D nanostructure arrays with the shapes of nanowires, nanonails, and nanotrees have been prepared by oxygen-assisted thermal evaporation of metallic zinc on quartz substrates [129]. The authors suggested that the formation of 1D nanostructures is governed by a self-catalyzed vapor-liquid-solid approach. The sensitivity of this material to CO was studied by monitoring the change of its resistance in the temperature range 27–317°C. It was found that when the film is exposed to 200 ppm of CO at 225°C, its resistance decreases by a factor of ~1.7. Response and recovery times are a few minutes. Sensor response is suggested to be based on the CO oxidation reaction:

$$2CO + O_2^- = 2CO_2 + e^- \tag{19}$$

Sensors based on nanonails and nanotrees are not CO-specific. They react to 200 ppm of NO_2 at 225°C, and to 100 ppm of H_2S at 100°C [129]. The influence of temperature on CO sensitivity was studied on an example of Cu-doped ZnO thin films [53]. The films were vacuum-deposited on glass substrates at a temperature of 150°C.

3.4. Detection of Nitrogen Oxides

Large amounts of nitrogen oxides are produced by motor vehicles. Other sources are electric utilities and other industrial, commercial, and residential sources that burn fuels. The need for NO_x sensor development is explained by environmental factors. The NO_x gases can cause various problems such as smog and acid rain. Thus, sensors are needed for environmental monitoring and for use in cars to control the combustion process. Several recent examples of development of new sensor materials to detect nitrogen oxides are presented in Table 5.

The NO_x sensors for automotive applications should detect levels of NO in range of 100–2,000 ppm and NO_2 in the range of 20–200 ppm in the presence of 1–10% of O_2 at temperatures ~400°C or above. Thus, the problems of sensitivity, selectivity, and stability must be addressed when developing such materials.

Table 5. Some recent papers on detection of nitrogen oxides.

Material	Analyte	Concentration	Temperature (°C)	Ref.
ZnO	NO	1000 ppm	200	[91]
SnO_2:WO_3	NO_2	500 ppm	150	[130]
ZnO:In	NO_2	5 ppm	275	[131]
ZnO	NO_2	1 ppm	300–350	[132]
ZnO	NO_2	1 ppm	300	[133]
SnO_2/SWCNT	NO_2	5–60 ppm	150	[134]
SnO_2:Zn	NO_2, NO_x	0.1–5 ppm	100–500	[135]
ZnO:Al	NO_x	20 ppm	100	[136]
ZnO:In_2O_3/WO_2	NO_x	10 ppm	150	[137]
WO_2/TiO_2:Pt	NO_x	10–570 ppm	570	[138]

3.5. Detection of Hydrogen

Analytical and sensor detection of hydrogen is of practical importance. On one hand, this is due to the increasing use of hydrogen as an ecologically clean fuel. On the other hand, it is well known that mixtures of hydrogen and oxygen are explosive. Hydrogen leaks must be carefully controlled in nuclear power plants and in the chemical industry.

Metal oxides, and particularly ZnO, are used for hydrogen detection. Some recent papers are presented in Table 6. Two successful research directions are being developed. One is connected with using oxides doped with metal particles, which possess catalytic properties for hydrogenation reactions. Palladium and platinum metals are the most often used metals. Another direction is connected with modification of oxides prepared by various methods. A combination of these approaches is also used.

The sensitivity to hydrogen of undoped and Pd-doped zinc oxide nanorods were compred and the results, obtained on ZnO thin films, were reported [144]. The sensitivity was measured by the resistance change at room temperature in the hydrogen concentration range 10–500 ppm. Hydrogen was mixed with air, and it was found that the in the absence of Pd, ZnO possesses low sensitivity to H_2. Doping by sputter-deposited Pd clusters can increase the sensitivity of material by approximately a factor of five. This fact is explained by promoting the catalytic dissociation of hydrogen. No response was detected to the presence of O_2 in ambient air. The response time was greater than 15 min, but recovery was rapid (less than 20 s).

The sensitivities for detecting hydrogen with Pt-coated single ZnO nanorods and thin films of various thicknesses (20–350 nm) were compared. It was found that the response of Pt-coated single ZnO nanorods is approximately a factor of three larger upon exposure to 500 ppm of H_2 in N_2 than that of zinc oxide thin films at room temperature. The power consumption of both types of sensors can be very low. The nanorod sensors exhibit faster response but slower recovery than the ZnO thin films, which is consistent with relatively higher adsorption ability at the nanorod's surface. The poorer current stability of single nanorod sensor devices in comparison with multiple nanorod sensors is reported.

High hydrogen sensitivity was demonstrated on vertically-aligned ZnO nanorods, synthesized by hydrothermal technique at 90°C on a Si(100) substrate [145]. The sensitivity of material was investigated at room temperature and dry air at a total flow rate of 500 sccm. The diameter of ZnO nanorods varied from 20 to 100 nm and the length was several hundreds nanometers. Hydrogen concentrations in range 20–200 ppm were used. The size effect of the ZnO nanorods on gas sensing properties were studied by comparison with nanorods of 500 nm in diameter. It was found that for detection of 200 ppm of hydrogen at 250°C the sensitivity of narrow nanorods was approximately four times larger than the sensitivity of 500 nm diameter nanorods achieved at 350°C. Response time was 800 s and recovery time was 200 s. It is reported that the sensitivity of the device can be empirically represented as $S = 1 + A_g(P_g)^{\beta}$, where P_g is the target gas partial pressure, which is proportional to gas concentration, A_g is a prefactor and β is the exponent on P_g. The value of β is derived from the surface interaction between chemisorbed oxygen anions and reducing gas and it should be close to 0.5 for uniform and ordered structures [145].

Table 6. Some recent papers on detection of hydrogen.

Material	Analyte	Concentration	Temperature (°C)	Ref.
ZnO	H_2	0.06%	300–400	[132]
SnO_2:Pd	H_2	0.50%	Room temp.	[139]
SnO_2:Pd	H_2	1,000 ppm	300	[140]
ZnO	H_2	10–2,500 ppm	350	[103]
ZnO	H_2	250 ppm	20	[141]
SnO_2:F	H_2	100 ppm	320	[142]
SnO_2–Ag_2O–PtO_x	H_2	100 ppm	125	[110]
SnO_2:Pd	H_2	1 ppm	150	[143]

Table 7. Some recent papers on detection of ammonia.

Material	Analyte	Concentration	Temperature (°C)	Ref.
SnO_2/MWCNT	NH_3	60–800 ppm	Room temp.	[148]
SnO_2:MoO_3,Fe_2O_3	NH_3	500 ppm	350	[149]
ZnO	NH_3	40–1,000 ppm	900	[150]
ZnO:Cr_2O_3	NH_3	300 ppm	20	[151]
ZnO:ZnS, CdS	NH_3	30 ppm	20	[152]
ZnO	NH_3	10–500 ppm	20	[144]
SnO_2:Pd	NH_3	100 ppm	300–500	[153]
SnO_2/SWCNT	NH_3	10 ppm	Room temp.	[154]
ZnO	NH_3	10 ppm	170	[116]
WO_3:Ti	NH_3	5–400 ppm	200	[155]

3.6. Detection of Ammonia

Ammonia is a toxic gas that is naturally present in the atmosphere in sub-ppb levels. However, much larger concentrations can be detected near farms with domestic animals. A large amount of ammonia is produced by the chemical industry for the production of fertilizers or for use in refrigeration systems. Ammonia sensors are needed for the early detection of possible leakages from such systems.

Another field of application is medicine, since the increase of amount of ammonia contained in exhaled air can be connected with certain diseases, including kidney disorders [146] and ulcers caused by *Helicobacter pylori*. A comprehensive review on different types of ammonia sensors has been published elsewhere [147]. Several of the latest results are presented in Table 7.

Remarkable results are obtained on systems, including SnO_2 with single wall carbon nanotubes (SWCNTs) or multi-wall carbon nanotubes (MWCNTs), which allow detection of low concentrations of ammonia at room temperature. Systematic investigations of doping WO_3 with 48 different metals have been carried out [156, 157]. For doping, 1 wt% of each additive was used. The best increase of sensitivity to ammonia was observed for Er- and Ga-doped WO_3 material. In another work a particularly good response to ammonia was observed for Cr-doped WO_3 sensor [153].

Table 8. Some recent papers on detection of other gases and VOCs.

Material	Analyte	Concentration	Temperature (°C)	Ref.
SnO_2	$(C_2H_5)_3N$	1 ppm	350	[158]
SnO_2	$(C_2H_5)_3N$	1 ppb	150	[159]
ZnO	$(CH_3)_3N$	10 ppm	170	[116]
SnO_2:Pd	Acetone	200 ppm	400	[160]
ZnO	Acetone	10 ppm	170	[116]
SnO_2:La_2O_3	C_2H_4O	20 ppm	250–300	[161]
ZnO	H_2S	12 ppm	300	[133]
ZnO	H_2S	100–300 ppm	Room temp.	[162]
SnO_2:CuO	H_2S	10 ppm	Room temp.	[163]
SnO_2:Ag	H_2S	1 ppm	70	[164]
ZnO	H_2S	0.01 ppm	150	[165]
ZnO	H_2S	ppb	20	[100]
ZnO	LPG	0.4%	578	[166]
ZnO	LPG	0.2%	400	[32]
ZnO	LPG	0.2%	400	[167]
SnO_2:Ni	LPG	600 ppm	350	[168]
ZnO:Pd	LPG	10%	170	[169]
SnO_2:Sr	LPG	10 ppm	210–300	[170]
SnO_2:V	SO_2	5 ppm	350	[171]
SnO_2:CuO, WO_3	Toluene	30 ppm	175	[172]

3.7. Detection of Other Gases

The remarkable results obtained recently for metal-oxide materials for detection of other toxic or flammable gases and VOCs, such as alkylamines, acetone, formaldehyde, hydrogen sulfide, liquified petroleum gas (LPG), sulfur dioxide and toluene are presented in Table 8.

4. CONCLUSIONS AND FUTURE DIRECTIONS

The considered applications and particular features of metal-oxide gas sensors allow us to formulate some general trends in this actively developing field of science.

- There is a clear tendency to search for new types of metal oxide nanostructures, including nanowires, nanobelts, and nanorods that promote the use of new synthetic techniques for preparation of novel sensor materials.
- There has been an increase in the number of different dopants, particularly various metal and metal oxide nanoparticles and substrate materials. These approaches are aimed at increasing the sensitivity and selectivity of metal-oxide gas sensors.
- Much effort is being made to extend the working temperature range of metal-oxide gas sensors and lower the optimal working temperature to 20–25°C. The goal of these investigations is to decrease the power consumption of sensor elements.

The analysis of available papers on sensor applications of metal-oxide nanostructures enables the formulation of a number of tasks that will draw the main efforts of scientists and engineers working on gas sensing nanomaterials in near future. At the moment little attention has been paid to the surface modification of sensor materials; hence, more efforts are needed on this topic. Moreover, the chemistry of metal and metal oxide nanoparticles and their peculiarities and size effects have also been reviewed in recently published books [173, 174]. However, the reactivity of doped metal oxides is currently under-investigated. The *in situ* spectroscopic studies of sensor materials at real working conditions are still quite rear.

Detailed theoretical and experimental investigations are needed for deep understanding of possible physical and chemical processes in real systems, involving metal oxides, dopants, analytes and various other molecules, such as water, which may be present in the atmosphere in target applications. This understanding can help in solving the problems with sensitivity, selectivity, and stability of sensor materials. One prospective approach is to chemically modify the surface of metal dopant particles with appropriate ligands to increase the specificity of sensor.

From a practical point of view, the problem of sensor stability deserves more attention than it has now. It is also necessary to test the real sensor working conditions for several days. Higher stability will decrease the frequency of or completely eliminate the need for verification and re-calibration of sensors. Another important problem is the development of simpler sensor materials and cheaper preparation methods.

In our opinion, new perspectives of using metal oxides for gas sensor materials lie not only in the field of new shapes and decrease of size of basic elements, but also in the application of composites involving metal oxides, metals, and various organic and inorganic ligands. Creation of new sensitive, selective, and stable gas sensor materials is one of the most important and actual tasks of nanochemistry and nanotechnology.

ACKNOWLEDGMENTS

The financial support of RFBR grant 08-03-00712 is acknowledged.

REFERENCES

1. A. Hulanicki, S. Glab, and F. Ingman, *Pure & Appl. Chem.* 63, 1247 (1991).
2. P. Gründler, "Chemical Sensors: An Introduction for Scientists and Engineers." Springer, Berlin, 2007.
3. W. H. Brattain and J. Bardeen, *Bell. Syst. Tech. J.* 32, 1 (1953).

4. T. Seiyama, A. Kato, K. Fujiishi, and M. Nagatani, *Anal. Chem.* 34, 1502 (1962).
5. N. Yamazoe and N. Miura, "Chemical Sensor Technology" (S. Yamauchi, Ed.), Vol. 4, p. 19. Kodansha, Tokyo, 1992.
6. H. Meixner and U. Lampe, *Sens. Actuators, B* 33, 198 (1996).
7. V. E. Bochenkov and G. B. Sergeev, *Adv. Coll. Int. Sci.* 116, 245 (2005).
8. L. Fu, L. Cao, Yu. Liu, and D. Zhu, *Adv. Coll. Int. Sci.* 111, 133 (2004).
9. V. E. Bochenkov and G. B. Sergeev, *Russ. Chem. Rev.* 76, 1013 (2007).
10. G. Jiménez-Cadena, J. Riu, and F. X. Rius, *The Analyst* 132, 1083 (2007).
11. I. Simon, N. Bârsan, M. Bauer, and U. Weimar, *Sens. Actuators, B* 73, 1 (2001).
12. M. Iwamoto, "Chemical Sensor Technology" (S. Yamauchi, Ed.), Vol. 4, p. 63. Kodansha, Tokyo, 1992.
13. N. Bârsan and U. Weimar, *J. Electroceramics.* 7, 143 (2001).
14. N. Bârsan, M. Schweizer-Berberich, and W. Göpel, *Fresenius J. Anal. Chem.* 365, 287 (1999).
15. M. J. Madou and S. R. Morrison, "Chemical Sensing with Solid State Devices." Academic Press, London, 1991.
16. T. Wolkenstein, "Electronic Processes on Semiconductor Surfaces During Chemisorption." Consultants Bureau, New York, 1991.
17. I. Kocemba, *Electron Technology* 29, 372 (1996).
18. G. Bläser, Th. Rühl, C. Diehl, M. Ulrich, and D. Kohl, *Physica A* 266, 218 (1999).
19. J. P. Santos and J. A. Agapito, *Thin Solid Films* 338, 276 (1999).
20. J. Watson, *Sens. Actuators, B* 8, 173 (1992).
21. C. Malagù, V. Guidi, M. Stefancich, M. C. Carotta, and G. Martinelli, *J. Appl. Phys.* 91, 808 (2002).
22. M. C. Carotta, A. Giberti, V. Guidi, C. Malagù, B. Vendemiati, and G. Martinelli, "Mater. Res. Soc. Symp. Proc.," 2005, Vol. 828, p. A4.6.1.
23. C. Malagù, M. C. Carotta, S. Galliera, V. Guidi, T. G. G. Maffeis, G. Martinelli, G. T. Owen, and S. P. Wilks, *Sens. Actuators, B* 103, 50 (2004).
24. R. C. Aiyer, S. G. Ansari, P. Boroojerdian, R. N. Karekar, S. K. Kulkarni, and S. R. Sainkar, *Thin Solid Films* 295, 271 (1997).
25. A. Gurlo, M. Ivanovskaya, N. Bârsan, M. Sweizer-Berberich, U. Weimar, W. Göpel, and A. Diéguez, *Sens. Actuators, B* 44, 327 (1997).
26. O. K. Tan, W. Zhu, Q. Yan, and L. B. Kong, *Sens. Actuators, B* 65, 361 (2000).
27. C. R. Michel, E. Lopéz-Mena, and A. H. Martinez, *Talanta* 74, 235 (2007).
28. M. K. Kennedy, F. E. Kruis, H. Fissan, B. R. Mentha, S. Stappert, and G. Dumpich, *J. Appl. Phys.* 93, 551 (2003).
29. E. V. Shmanova, V. E. Bochenkov, V. V. Zagorsky, and G. B. Sergeev, *Mendeleev Commun.* 18, 8 (2008).
30. Y. Shimizu, T. Hyodo, and M. Egashira, *J. Eur. Cer. Soc.* 24, 1389 (2004).
31. M. Egashira, Y. Shimizu, and T. Hyodo, "Mater. Res. Soc. Symp. Proc.," 2005, Vol. 828, p. A1.1.1.
32. V. R. Shinde, T. P. Gujar, and C. D. Lokhande, *Sens. Actuators, B* 123, 701 (2007).
33. H. Xu, X. Liu, D. Cui, M. Li, and M. Jiang, *Sens. Actuators, B* 114, 301 (2006).
34. Y. Shen, T. Yamazaki, Z. Liu, C. Jin, T. Kikuta, and N. Nakatani, *Thin Solid Films* 516, 5111 (2008).
35. E. Comini, G. Faglia, G. Sberveglieri, Z. Pan, and Z. L. Wang, *Appl. Phys. Lett.* 81, 1869 (2002).
36. I. Z. Rahman, K. M. Razeeb, M. A. Rahman, and Md. Kamruzzaman, *J. Magn. Mat. Mater.* 262, 166 (2003).
37. E. Comini, V. Guidi, C. Malagù, G. Martinelli, Z. Pan, G. Sberveglieri, and Z. Wang, *J. Phys. Chem.* 108, 1882 (2004).
38. A. Kolmakov and M. Moskovits, *Annu. Rev. Mater. Res.* 34, 151 (2004).
39. X.-J. Huang and Y.-K. Choi, *Sens. Actuators, B* 122, 659 (2007).
40. Y. Xia, Y. Yang, P. Sun, Y. Wu, B. Mayers, B. Gates, Y. Yin, F. Kim, and H. Yan, *Adv. Mater.* 15, 353 (2003).
41. W. Gu, H. Choi, and K. Kim, *Appl. Phys. Lett.* 89, 253102 (2006).
42. A. Kolmakov, Y. X. Zhang, G. S. Cheng, and M. Moskovits, *Adv. Mater.* 15, 997 (2003).
43. Y. L. Wang, X. C. Jiang, and Y. N. Xia, *J. Am. Chem. Soc.* 125, 16176 (2003).
44. F. Fernández-Ramirez, A. Tarancón, O. Casals, J. Arbiol, A. Romano-Rodriguez, and J. R. Morante, *Sens. Actuators, B* 121, 3 (2007).
45. Z. L. Wang, *Annu. Rev. Phys. Chem.* 55, 159 (2004).
46. S. Dmitriev, Y. Lilach, B. Button, M. Moskovits, and A. Kolmakov, *Nanotechnology* 18, 1 (2007).
47. T. B. Fryberger and S. Semancik, *Sens. Actuators, B* 2, 305 (1990).
48. S. Semancik and T. B. Fryberger, *Sens. Actuators, B* 1, 97 (1990).
49. L. Madler, A. Roessler, S. E. Pratsinis, T. Sahm, A. Gurlo, N. Barsan, and U. Weimar, *Sens. Actuators, B* 114, 283 (2006).
50. U.-S. Choi, G. Sakai, K. Shimanoe, and N. Yamazoe, *Sens. Actuators, B* 107, 397 (2006).
51. O. Wurzinger and G. Reinhardt, *Sens. Actuators, B* 103, 104 (2006).
52. R. K. Joshi, F. E. Kruis, and O. Dmitrieva, *J. Nanopart. Res.* 8, 797 (2006).
53. J. Gong, Q. Chen, M. R. Lian, N. C. Liu, R. G. Stevenson, and F. Adami, *Sens. Actuators, B* 114, 32 (2006).
54. A. Galdikas, A. Mironas, and A. Setkus, *Sens. Actuators, B* 26, 29 (1995).
55. S. B. Patil, M. A. Patil, and P. P. More, *Sens. Actuators, B* 125, 126 (2007).
56. C. H. Han, D. U. Hong, J. Gwak, and S. D. Han, *Kor. J. Chem. Eng.* 24, 927 (2007).
57. C. Xu, J. Tamaki, N. Miura, and N. Yamazoe, *Sens. Actuators, B* 3, 147 (1991).
58. M. Gaidi, M. Labeau, B. Chenevier, and J. L. Hazemann, *Sens. Actuators, B* 48, 277 (1998).
59. S. C. Tsang, C. D. A. Bulpitt, P. C. H. Mitchell, and A. J. Ramirez-Cuesta, *J. Phys. Chem. B* 105, 5737 (2001).

60. A. Cabot, A. Diéguez, A. Romano-Rodríguez, J. R. Morante, and N. Bârsan, *Sens. Actuators, B* 79, 98 (2001).
61. S. Manorama, G. Sarala Devi, and V. J. Rao, *Appl. Phys. Lett.* 64, 3163 (1994).
62. M. N. Rumyantseva, M. Labeau, J. P. Senateur, G. Delabouglise, M. N. Boulova, and A. M. Gaskov, *J. Mater. Sci. Eng. B* 41, 228 (1996).
63. M. Rumyantseva, M. Labeau, G. Delabouglise, L. Ryabova, I. Kutsenok, and A. Gaskov, *J. Mater. Chem.* 7, 1785 (1997).
64. R. B. Vasiliev, M. N. Rumyantseva, N. V. Yakovlev, and A. M. Gaskov, *Sens. Actuators, B* 50, 186 (1998).
65. A. Chowdhuri, P. Sharma, V. Gupta, K. Sreenivas, and K. V. Rao, *J. Appl. Phys.* 92, 2172 (2002).
66. W. Yuanda, T. Maosong, H. Xiuli, Z. Yushu, and D. Guorui, *Sens. Actuators, B* 79, 187 (2001).
67. V. V. Kissine, S. A. Voroshilov, and V. V. Sysoev, *Thin Solid Films* 348, 304 (1999).
68. S. Chakraborty, A. Sen, and H. S. Maiti, *Sens. Actuators, B* 115, 610 (2006).
69. F. Parret, Ph. Ménini, A. Martinez, K. Soulantica, A. Maisonnat, and B. Chaudret, *Sens. Actuators, B* 118, 276 (2006).
70. S. Nakata, H. Okunishi, and Y. Nakashima, *Sens. Actuators, B* 119, 556 (2006).
71. S. Nakata, H. Okunishi, and Y. Nakashima, *Analyst* 131, 148 (2006).
72. J. R. Huang, G. Y. Li, Z. Y. Huang, X. J. Huang, and J. H. Liu, *Sens. Actuators, B* 114, 1059 (2006).
73. J. R. Huang, C. P. Gu, F. L. Meng, M. Q. Li, and J. H. Liu, *Smart Mater. Struct.* 16, 701 (2007).
74. P. Heszler, R. Ionescu, E. Llobet, L. F. Reyes, J. M. Smulko, L. B. Kish, and C. G. Granqvist, *Phys. Status Solidi B* 244, 4331 (2007).
75. A. Baschirotto, S. Capone, A. D'Amico, C. Di Natale, V. Ferragina, G. Ferri, L. Francioso, M. Grassi, N. Guerrini, P. Malcovati, E. Martinelli, and P. Siciliano, *Sens. Actuators, B* 130, 164 (2008).
76. V. V. Sysoev, J. Goschnick, T. Schneider, E. Strelcov, and A. Kolmakov, *Nano Lett.* 7, 3182 (2007).
77. F. Röck, N. Barsan, and U. Weimar, *Chem. Rev.* 108, 705 (2008).
78. S. Ahlers, G. Muller, and T. Doll, *Sens. Actuators, B* 107, 587 (2005).
79. S. Wlodek, K. Colbow, and F. Consadori, *Sens. Actuators, B* 3, 123 (1991).
80. W. M. Sears, K. Colbow, and F. Consadori, *Sens. Actuators, B* 19, 333 (1989).
81. A. Vergara, E. Llobet, J. Brezmes, P. Ivanova, C. Cané, I. Gràcia, X. Vilanova, and X. Correig, *Sens. Actuators, B* 123, 1002 (2007).
82. B. Panchapakesan, R. Cavicchi, S. Semancik, and D. L. Devoe, *Nanotechnology* 17, 415 (2006).
83. P. Lv, Z. Tang, G. Wei, J. Yu, and Z. Huang, *Meas. Sci. Technol.* 18, 2997 (2007).
84. E. Comini, G. Faglia, and G. Sberveglieri, "Proceedings of SPIE-The International Society for Optical Engineering," 2004, Vol. 5275, p. 1.
85. A. Adami, L. Lorenzelli, V. Guarnieri, L. Francioso, A. Forleo, G. Agnusdei, A. M. Taurino, M. Zen, and P. Siciliano, *Sens. Actuators, B* 117, 115 (2006).
86. S. Ampuero and J. O. Bosset, *Sens. Actuators, B* 94, 1 (2003).
87. P. Bhattacharyya, P. K. Basu, H. Saha, and S. Basu, *Sensor Lett.* 4, 371 (2006).
88. A. Wisitsoraat, A. Tuantranont, C. Thanachayanont, V. Patthanasettakul, and P. Singjai, *J. Electroceram.* 17, 45 (2006).
89. J. T. McCue and J. Y. Ying, *Chem. Mater.* 19, 1009 (2007).
90. T. Ueda, V. V. Plashnitsa, M. Nakatou, and N. Miura, *Electrochem. Commun.* 9, 197 (2007).
91. H. J. Lim, D. Y. Lee, and Y. J. Oh, *Sens. Actuators, A* 125, 405 (2006).
92. G. Socol, E. Axente, C. Ristoscu, F. Sima, A. Popescu, N. Stefan, I. N. Mihailescu, L. Escoubas, J. Ferreira, S. Bakalova, and A. Szekeres, *J. Appl. Phys.* 102, 083103 (2007).
93. A. Og. Dikovska, P. A. Atanasov, S. Tonchev, J. Ferreira, and L. Escoubas, *Sens. Actuators, A* 140, 19 (2007).
94. N. H. Kim and G. J. Kim, *J. Nanosci. Nanotechnol.* 7, 3914 (2007).
95. P. Bhattacharyya, P. K. Basu, H. Saha, and S. Basu, *Sens. Actuators, B* 124, 62 (2007).
96. P. Bhattacharyya, P. K. Basu, N. Mukherjee, A. Mondal, H. Saha, and S. Basu, *J. Mater. Sci.-Mater. Electron.* 18, 823 (2007).
97. Y. Pimtong-Ngam, S. Jiemsirilers, and S. Supothina, *Sens. Actuators, A* 139, 7 (2007).
98. P. Bhattacharyya, P. K. Basu, C. Lang, H. Saha, and S. Basu, *Sens. Actuators, B* 129, 551 (2008).
99. D. Kohl, *J. Phys. D* 34, R125 (2001).
100. S. Wang, Y. Zhao, J. Huang, Y. Wang, S. Wu, S. Zhang, and W. Huang, *Solid-State Electron.* 50, 1728 (2006).
101. G. Neri, A. Bonavita, G. Micali, N. Donato, F. A. Deorsola, P. Mossino, I. Amato, and B. De Benedetti, *Sens. Actuators, B* 117, 196 (2006).
102. A. Og. Dikovska, P. A. Atanasov, T. R. Stoyanchov, A. T. Andreev, E. I. Karakoleva, and B. S. Zafirova, *Appl. Opt.* 46, 2481 (2007).
103. L. J. Bie, X. N. Yan, J. Yin, Y. Q. Duan, and Z. H. Yuan, *Sens. Actuators, B* 126, 604 (2007).
104. T. J. Hsueh, Y. W. Chen, S. J. Chang, S. F. Wang, C. L. Hsu, Y. R. Lin, T. S. Lin, and I. C. Chen, *J. Electrochem. Soc.* 154, J393 (2007).
105. S. M. Chou, L. G. Teoh, W. H. Lai, Y. H. Su, and M. H. Hon, *Sensors* 6, 1420 (2006).
106. X. Li, X. L. He, J. P. Li, and Y. Zhang, *Chin. J. Sens. Actuators* 20, 2169 (2007).
107. C. Liewhiran and S. Phanichphant, *Sensors* 7, 1159 (2007).
108. C. Liewhiran, A. Camenzind, A. Teleki, S. E. Pratsinis, and S. Phanichphant, "Proceedings of the 2nd IEEE International Conference on Nano/Micro Engineered and Molecular Systems, IEEE NEMS" (2007), p. 672.
109. F. Pourfayaz, Y. Mortazavi, A. Khodadadi, and S. Ajami, *Sens. Actuators, B* 130, 625 (2008).
110. I. J. Kim, S. D. Han, C. H. Han, J. Gwak, D. U. Hong, D. Jakhar, K. C. Singh, and J. S. Wang, *Sens. Actuators, B* 127, 441 (2007).

111. L. M. Li, C. C. Li, J. Zhang, Z. F. Du, B. S. Zou, H. C. Yu, Y. G. Wang, and T. H. Wang, *Nanotechnology* 18, 225504 (2007).
112. C. Liewhiran and S. Phanichphant, *Sensors* 7, 650 (2007).
113. C. Ge, C. Xie, and S. Cai, *Mater. Sci. Eng. B* 137, 53 (2007).
114. J. J. Delaunay, N. Kakoiyama, and I. Yamada, *Mater. Chem. Phys.* 104, 141 (2007).
115. J. J. Delaunay, N. Kakoiyama, and I. Yamada, "Proceedings of SPIE-The International Society for Optical Engineering," 2006, Vol. 6122, p. 612208.
116. R. L. Liu, Q. Xiang, Q. Y. Pan, Z. X. Cheng, L. Y. Shi, and W. C. Xuebao, *J. Inorg. Mater.* 21, 793 (2006).
117. K. Arshak, E. Moore, C. Cunniffe, M. Nicholson, and A. Arshak, *Superlattices Microstruct.* 42, 479 (2007).
118. H. Tang, Y. Li, C. Zheng, J. Ye, X. Hou, and Y. Lv, *Talanta* 72, 1593 (2007).
119. L. Liao, H. B. Lu, J. C. Li, H. He, D. F. Wang, D. J. Fu, C. Liu, and W. F. Zhang, *J. Phys. Chem. C* 111, 1900 (2007).
120. C. Liewhiran and S. Phanichphant, *Sensors* 7, 185 (2007).
121. J. J. Delaunay, K. Yanagisawa, T. Nishino, and I. Yamada, "Proceedings of SPIE-The International Society for Optical Engineering," 2007, Vol. 6413, p. 641304.
122. T. Anukunprasert, C. Saiwan, E. Di Bartolomeo, and E. Traversa, *J. Electroceram.* 18, 295 (2007).
123. J. X. Wang, X. W. Sun, S. S. Xie, Y. Yang, H. Y. Chen, G. Q. Lo, and D. L. Kwong, *J. Phys. Chem. C* 111, 7671 (2007).
124. J. L. González-Vidal, M. De La, L. Olvera, A. Maldonado, A. Reyes-Barranca, and M. Melendez-Lira, *Rev. Mex. Fis.* 52, 6 (2006).
125. J. X. Wang, X. W. Sun, H. Huang, Y. C. Lee, O. K. Tan, M. B. Yu, G. Q. Lo, and D. L. Kwong, *Appl. Phys. A* 88, 611 (2007).
126. L. H. Qian, K. Wang, Y. Li, H. T. Fang, Q. H. Lu, and X. L. Ma, *Mater. Chem. Phys.* 100, 82 (2006).
127. L. Maedler, T. Sahm, A. Gurlo, J. D. Grunwaldt, N. Barsan, U. Weimar, and S. E. Pratsinis, *J. Nanopart. Res.* 8, 783 (2006).
128. P. Samarasekara, N. U. S. Yapa, N. T. R. N. Kumara, and M. V. K. Perera, *Bull. Mater. Sci.* 30, 113 (2007).
129. S. Kar, B. N. Pal, S. Chaudhuri, and D. Chakravorty, *J. Phys. Chem. B* 110, 4605 (2006).
130. J. Kaur, S. C. Roy, and M. C. Bhatnagar, *Sens. Actuators, B* 123, 1090 (2007).
131. R. Ferro, J. A. Rodriguez, P. Bertrand, M. Henry, and C. Poleunis, *Rev. Mex. Fis.* 52, 23 (2006).
132. A. Z. Sadek, S. Choopun, W. Wlodarski, S. J. Ippolito, and K. Kalantar-zadeh, *IEEE Sens. J.* 7, 919 (2007).
133. C. M. Ghimbeu, J. Schoonman, M. Lumbreras, and M. Siadat, *Appl. Surf. Sci.* 253, 7483 (2007).
134. J. Lu, A. Ma, S. Yang, and K. M. Ng, *J. Nanosci. Nanotechnol.* 7, 1589 (2007).
135. A. Sutti, C. Baratto, G. Calestani, C. Dionigi, M. Ferroni, G. Faglia, and G. Sberveglieri, *Sens. Actuators, B* 130, 567 (2008).
136. S. C. Navale, V. Ravi, I. S. Mulla, S. W. Gosavi, and S. K. Kulkarni, *Sens. Actuators, B* 126, 382 (2007).
137. C. S. Rout, K. Ganesh, A. Govindaraj, and C. N. R. Rao, *Appl. Phys. A* 85, 241 (2006).
138. K. I. Shimizu, K. Kashiwagi, H. Nishiyama, S. Kakimoto, S. Sugaya, H. Yokoi, and A. Satsuma, *Sens. Actuators, B* 130, 707 (2008).
139. D. Ito and M. Ichimura, *Jpn. J. Appl. Phys., Part 1* 45, 7094 (2006).
140. T. Yamazaki, C. Jin, Y. Shen, T. Kikuta, and N. Nakatatani, *Materials Science Forum* 539–543, 3508 (2007).
141. J. Yang, G. Liu, J. Lu, Y. Qiu, and S. Yang, *Appl. Phys. Lett.* 90, 103109 (2007).
142. C. H. Han, S. D. Han, and S. P. Khatkar, *Sensors* 6, 492 (2006).
143. S. Dmitriev, "Materials Research Society Symposium Proceedings," 2006, Vol. 915, p. 203.
144. B. S. Kang, H. T. Wang, L. C. Tien, F. Ren, B. P. Gila, D. P. Norton, C. R. Abernathy, J. Lin, and S. J. Pearton, *Sensors* 6, 643 (2006).
145. H. C. Wang, Y. Li, and M. J. Yang, *Sens. Actuators, B* 119, 380 (2006).
146. L. R. Narasimhan, W. Goodman, C. Kumar, and N. Patel, *PNAS* 98, 4617 (2001).
147. B. Timmer, W. Olthuis, and A. van den Berg, *Sens. Actuators, B* 107, 666 (2005).
148. N. Van Hieu, L. T. B. Thuy, and N. D. Chien, *Sens. Actuators, B* 129, 888 (2008).
149. V. V. Kovalenko, A. A. Zhukova, M. N. Rumyantseva, A. M. Gaskov, V. V. Yushchenko, I. I. Ivanova, and T. Pagnier, *Sens. Actuators, B* 126, 52 (2007).
150. S. Wang, Y. Zhao, J. Huang, Y. Wang, F. Kong, S. Wu, S. Zhang, and W. Huang, *Vacuum* 81, 394 (2006).
151. D. R. Patil, L. A. Patil, and P. P. Patil, *Sens. Actuators, B* 126, 368 (2007).
152. N. Du, H. Zhang, B. Chen, J. Wu, and D. Yang, *Nanotechnology* 18, 115619 (2007).
153. A. M. Ruiz, X. Illa, R. Diáz, A. Romano-Rodriguez, and J. R. Morante, *Sens. Actuators, B* 118, 318 (2006).
154. N. D. Hoa, N. V. Quy, Y. S. Cho, and D. Kim, *Phys. Status Solidi A* 204, 1820 (2007).
155. M. Hu, C. Yong, Y. Feng, Y. Lv, L. Han, J. Liang, and H. Wang, "Proceedings of SPIE-The International Society for Optical Engineering," 2006, Vol. 6358 I, p. 635810.
156. C. N. Xu, N. Miura, Y. Ishida, K. Matsuda, and N. Yamazoe, *Sens. Actuators, B* 65, 163 (2000).
157. X. Wang, N. Miura, and N. Yamazoe, *Sens. Actuators, B* 66, 74 (2000).
158. D. Wang, X. Chu, and M. Gong, *Sens. Actuators, B* 117, 183 (2006).
159. W. Caihong, X. Chu, and M. Wu, *Sens. Actuators, B* 120, 508 (2007).
160. P. S. Cho, C. Y. Kang, S. J. Kim, J. S. Kim, S. J. Yoon, N. Van Hieu, and J. H. Lee, *Kor. J. Mater. Res.* 18, 69 (2008).
161. M. Kugishima, K. Shimanoe, and N. Yamazoe, *Sens. Actuators, B* 118, 171 (2006).
162. L. Liao, H. B. Lu, J. C. Li, C. Liu, D. J. Fu, and Y. L. Liu, *Appl. Phys. Lett.* 91, 173110 (2007).
163. L. A. Patil and D. R. Patil, *Sens. Actuators, B* 120, 316 (2006).

164. K. Shimanoe, S. Arisuda, K. Oto, and N. Yamazoe, *Electrochem.* 74, 183 (2006).
165. D. Wang, X. Chu, and M. Gong, *Nanotechnology* 18, 185601 (2007).
166. V. R. Shinde, T. P. Gujar, C. D. Lokhande, R. S. Mane, and S. H. Han, *Sens. Actuators, B* 123, 882 (2007).
167. V. R. Shinde, T. P. Gujar, and C. D. Lokhande, *Sens. Actuators, B* 120, 551 (2007).
168. K. Jain, R. P. Pant, and S. T. Lakshmikumar, *Sens. Actuators, B* 113, 823 (2006).
169. B. Baruwati, D. K. Kumar, and S. V. Manorama, *Sens. Actuators, B* 119, 676 (2006).
170. L. D. Feng, X. J. Huang, and Y. K. Choi, *Microchim. Acta* 156, 245 (2006).
171. S. Das, S. Chakraborty, O. Parkash, D. Kumar, S. Bandyopadhyay, S. K. Samudrala, A. Sen, and H. S. Maiti, *Talanta* 75, 385 (2008).
172. R. Z. Liu, Y. H. He, B. Wang, F. M. Liu, L. H. Chen, and B. F. Quan, *Chin. J. Sens. Actuators* 20, 267 (2007).
173. G. A. Ozin and A. C. Arsenault, "Nanochemistry. A Chemical Approach to Nanomaterials." RSC Publishing, London, 2005.
174. G. B. Sergeev, "Nanochemistry." Elsevier, Amsterdam, 2006.